Marine and Petroleum Geology 59 (2015) 491–504

Contents lists available at ScienceDirect

Marine and Petroleum Geology

journal homepage: www.elsevier.com/locate/marpetgeo

Review article

Heat-flow regimes and the hydrate stability zone of a transient, thermogenic, fault-controlled hydrate system (Woolsey Mound northern Gulf of Mexico)

L. Macelloni [a, *], C.B. Lutken [b], S. Garg [c], A. Simonetti [d], M. D'Emidio [b], R.M. Wilson [e], K. Sleeper [b], L.L. Lapham [f], T. Lewis [g], M. Pizzi [h], J.H. Knapp [d], C.C. Knapp [d], J. Brooks [i], T.M. McGee [b, †]

[a] National Institute of Undersea Science and Technology, University of Mississippi Field Station, University of Mississippi, University, MS 38677, USA
[b] Mississippi Mineral Resources Institute and Center for Marine Resources and Environmental Technology, University of Mississippi, 111 Brevard Hall, MS 38677, USA
[c] Leidos Inc., 10260 Campus Point Drive, M/S C2E, San Diego, CA 92121, USA
[d] Department of Earth and Ocean Sciences, University of South Carolina, 701 Sumter St., EWS Building, Columbia, SC 29208, USA
[e] EOAS-Oceanography, Florida State University, 117 N Woodward Ave, Tallahassee, FL 32306, USA
[f] Chesapeake Biological Lab, University of Maryland Center for Environmental Science, P.O. Box 38, 146 Williams St., Solomons, MD 20688, USA
[g] Sidney Geophysical Consultants, Ltd., 1107 Maple Road, N. Saanich, BC V8L 5P5, Canada
[h] Fugro Survey Limited (Great Yarmouth) Morton Peto Road Gapton Hall Industrial Estate, Great Yarmouth NR31 0LT, United Kingdom
[i] TDI-Brooks Int'l Inc., 1902 Pinon Dr., College Station, TX 77845, USA

ARTICLE INFO

Article history:
Received 13 May 2014
Received in revised form
1 September 2014
Accepted 15 September 2014
Available online 30 September 2014

Keywords:
Heat flow
Gas hydrate systems
Seafloor morphology, geology, and geophysics
Diapir and diapirism
Geochemical modeling

ABSTRACT

This study aims to constrain the base of the hydrates stability field in structurally complexsites using the case of Woolsey Mound, a fault-controlled, transient, thermogenic hydrates system, in Mississippi Canyon Block 118, northern Gulf of Mexico. We have computed the base of the hydrates stability field integrating results from a recent heat-flow survey, designed to investigate geothermal anomalies along fault zones which exhibit different fluid flux regimes. An advanced "compositional" simulator was used to model hydrate formation and dissociation at Woolsey Mound and addresses the following hypotheses:

1. Migrating thermogenic fluids alter thermal conditions of the Hydrate Stability Zone (HSZ), so heat-flow reflects fault activity;
2. Gas hydrate formation and dissociation vary temporally at active faults, temporarily sealing conduits for migration of thermogenic fluids;
3. High salinity and inclusion of thermogenic gases with higher molecular weight than methane produce opposite effects on the depth to the bottom of the hydrate stability zone.

Applications of results include identifying and quantifying hydrate deposits in shallow sediments using an interdisciplinary approach that includes multiple resolution seismic data evaluation, geological and geochemical groundtruthing and heat-flow analyses as a proxy for activity along faults.

1. Introduction

Marine gas hydrates occur on the continental shelves and slopes of the world, near the surface on polar shelves and buried in deep marine sediments in more southerly regions [Kvenvolden et al., 1993]. Stable under specific conditions of temperature, pressure, and salinity [Sloan and Koh, 2008], hydrates are frequently identified only through direct in situ measurement [Logging While Drilling, i.e. Cook et al., 2010; Collett et al., 2012] or inferred by seismic detection of bottom simulating reflectors [BSRs; i.e. Hyndman and Spence, 1992; Singh et al., 1993; Helgerud et al., 1999], indicators of the base of hydrate stability [Haacke et al., 2008].

* Corresponding author.
E-mail address: lmacello@olemiss.edu (L. Macelloni).
† Deceased.

http://dx.doi.org/10.1016/j.marpetgeo.2014.09.010
0264-8172/

The northern Gulf of Mexico continental slope presents a unique area for assessment of hydrates formation and dissociation in the framework of deep sea natural seeps. Abundant input of river sediments and differential loading mobilize massive salt bodies at depth. These processes generate complex systems of faults and fractures through which deep-sourced fluids and gases migrate and ultimately reach the seafloor in focused hydrocarbon vents [Brooks et al., 1986; MacDonald et al., 1994; Sassen et al., 2001], frequently associated with seafloor fluid-expulsion features (i.e. seafloor pockmarks, mud volcanoes) and gas hydrate deposits close to the seawater–sediment interface (hydrate mounds). In such complex settings, the portion of the hydrate stability zone (HSZ) that is actually occupied by hydrates, deviates markedly from the zone where solid methane hydrates are theoretically stable, marked by a clear phase boundary between solid gas hydrates and free gas (the classic BSR). Rather, this is a dynamic system that undergoes rapid change, and in which stability conditions are transient; free gas, gas hydrates and gas dissolved in pore fluids can coexist and/or free gas can pass without forming hydrates [Liu and Fleming, 2007]. The causes of the complex thermo-chemical regime of these sites is the concurrent action of multiple processes such as: 1) proximity to a salt body that inhibits the formation of hydrates [Taylor et al., 2000; Ruppel et al., 2005]; 2) laterally segmented geology [Andresen et al., 2011]; 3) transient advection along the conduits of thermogenic fluids and salt brines [Dewangan et al., 2011]; 4) molecules of hydrocarbon gases heavier than methane [Hornbach et al., 2005]. Therefore, there is a crucial need to measure/model heat flow, salinity saturation and fluids advection, in the plumbing system that sustains deep sea mounds, mud volcanoes and natural seeps to better understand hydrates stability\instability and ultimately constrain the volume of gas passing from the lithosphere to hydrosphere. To date a number of studies have tried to model the geothermal regimes in these settings worldwide. Where a seismically clear BSR is present, a BSR-derived2D/3D heat flow model can be used to derive the geothermal gradient i.e. Lüdmann et al., (2004) at the Black Sea; Vanneste et al., (2005) at the Svalbard margin; Hornbach et al., (2012) and Crutcheley et al., (2013) at the Hydrates Ridge (off shore Oregon); Hong-Li et al., (2014) at the Cucumber Ridge (off shore Vancouver Island). Where the seismic BSR is segmented, near/at the seafloor or even absent, such as in many areas of the Gulf of Mexico [Shedd et al., 2012], the geothermal gradient has been derived via heat probes in situ measurements [Ruppel et al., 2005; Hutchinson et al., 2009; Smith et al., 2014].

In this paper we present results of heat flow study at Woolsey Mound, a fault-controlled, transient, thermogenic hydrates system in the Northern Gulf of Mexico. We have computed the base of the hydrates stability field integrating the results from a high resolution in situ heat-flow survey that was specifically designed to investigate the geothermal regime along active fault zones where previous studies have recognized different fluid flux regimes [Lapham et al., 2008; Macelloni et al., 2013]. Furthermore, a "compositional" simulator, was developed especially to model the hydrate formation/dissociation of Structure II hydrates (formed by molecules heavier than methane). Considering Woolsey Mound a good analogue of sites worldwide that share the same genesis, our study aims to address, in particular, the following hypotheses: a) Gas hydrate formation and dissociation vary temporally; their formation can temporarily seal faults as conduits for thermogenic fluids and this will be reflected in heat-flow; b) Presence of thermogenic gases with higher molecular weight than methane can cause Structure II hydrates to form, and produce a vertically more extensive HSZ and diminishing the shoaling effect of high salinity.

1.1. Previous work at Woolsey Mound

Woolsey Mound, MC118, is the site of the Gulf of Mexico Hydrates Research Consortium's (GOMHRC) Seafloor Observatory [McGee, 2006], where the HSZ has been the subject of intense and continuing investigation since 2005 [Lutken et al., 2011a]. The one-kilometer-diameter carbonate/hydrate mound, located on the continental slope, in ~890 m water depth (Fig. 1) has been designated by the Bureau of Ocean Energy Management (BOEM), as the GOM's only Research Reserve.

Surface morphology at Woolsey Mound is characterized by three main crater clusters or complexes (Fig. 2), each 5–60 m in diameter and with bathymetric relief as high as 6 m. Macelloni et al., (2010) grouped the clusters into the SE, SW, and NW complexes based on bathymetric relief and the presence of seafloor features typical of cold seep systems.

Seismic records [Macelloni et al., 2012] place Woolsey Mound above a major salt body, the uppermost extent of which reaches to within 400 m of the seafloor. The mound appears to have evolved in close association with the crestal fault system developed above and around this dome-shaped salt body. Each crater complex is associated with a master fault: the NW complex with the blue and red faults, the SW complex with the magenta fault, and the SE complex with the yellow fault (Fig. 2).

Combining evidence from subsurface studies with seafloor surface observations, Macelloni et al., (2013) developed the conceptual model of the Woolsey Mound shown in Figure 3; this graphic portrays a multi-attributes (geology, biology, geochemistry, etc.) transect through the mound, and includes the three crater complexes. Hydrocarbon fluids (red arrows) migrate from the deep (thousands of meters) oil reservoir to the shallow subsurface via faults and fractures and accumulate in stratigraphic horizons that host high porosity sediments and/or fracture porosity. The Authors have found that this process is mainly controlled by the dynamics of two shallow gas horizons (indicated in Fig. 3 as BS-1 and BS-2) and by the hydraulic connection between them. The BS-2, which occupies the shallower stratigraphic position, seems to represent the base of hydrate stability at the Woolsey Mound. They hypothesize (dotted portion of the BHSZ yellow line in Fig. 3), that the stability field waxes and wanes, over time, along the faults.

2. Data and methods

2.1. Heat-flow survey

In March, 2012, a heat-flow survey was conducted for the GOMHRC by TDI-Brooks, International aboard the R/V *Geoexplorer*. Ultimately, fifteen sites, fourteen of which are plotted on the map of the seafloor backscatter in Figure 4, were selected to investigate the geothermal gradient across Woolsey Mound and the master faults. The sites were chosen as follow:

- calibration sites: UMH001 distant from the mound, in the south east corner of MC 161 (Fig. 1 Appendix A), UMH002 just outside the mound area in the north west corner of MC118
- pockmarks: UMH003, UMH004 and UMH015. UMH003 from the hanging wall of the blue fault, UMH004 from a lens-shaped pockmark near the red fault and UMH015 from a pock-mark at the surface terminus of the yellow fault
- suspected brine pool UMH008 (based on the seafloor biological communities observed there, Lutken et al., (2011b))
- transects that cross surface expressions of the master faults. Transect UMH005-007 crosses the blue fault with UMH005 on the hanging wall of the blue fault, and the vicinity from which hydrate was recovered in JPC-1 [Simonetti et al., 2013] as well as near the site of a marked resistivity anomaly noted in 2009 [Dunbar et al., 2010]; UMH006 is located in the blue fault and UMH007 on the footwall of the blue fault; transect UMH009-011 crosses the magenta fault with UMH011 being the site where

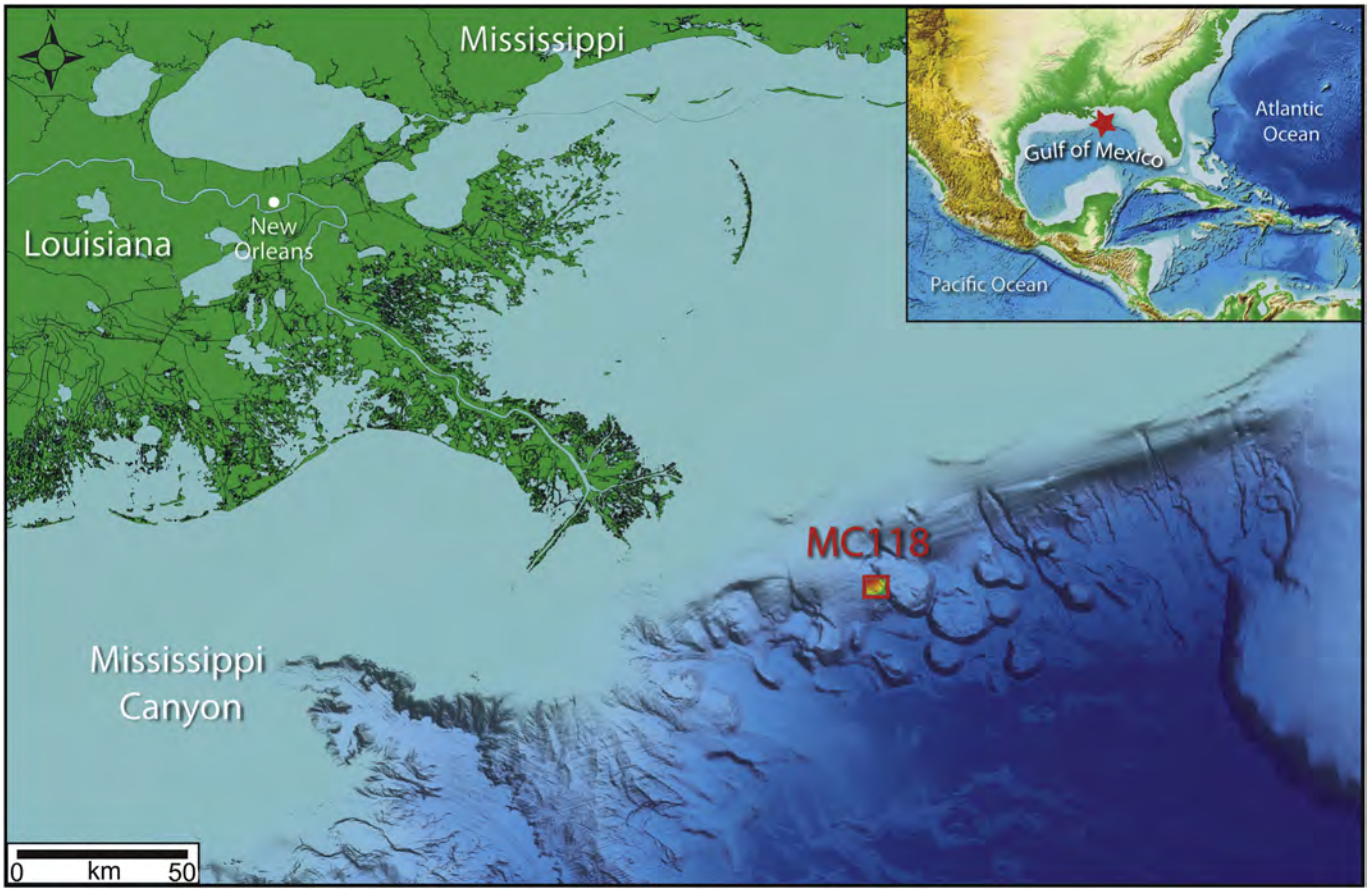

Figure 1. Woolsey Mound is located within Mississippi Canyon Lease Block 118, on the Northern Gulf of Mexico continental slope, an area of active salt tectonism.

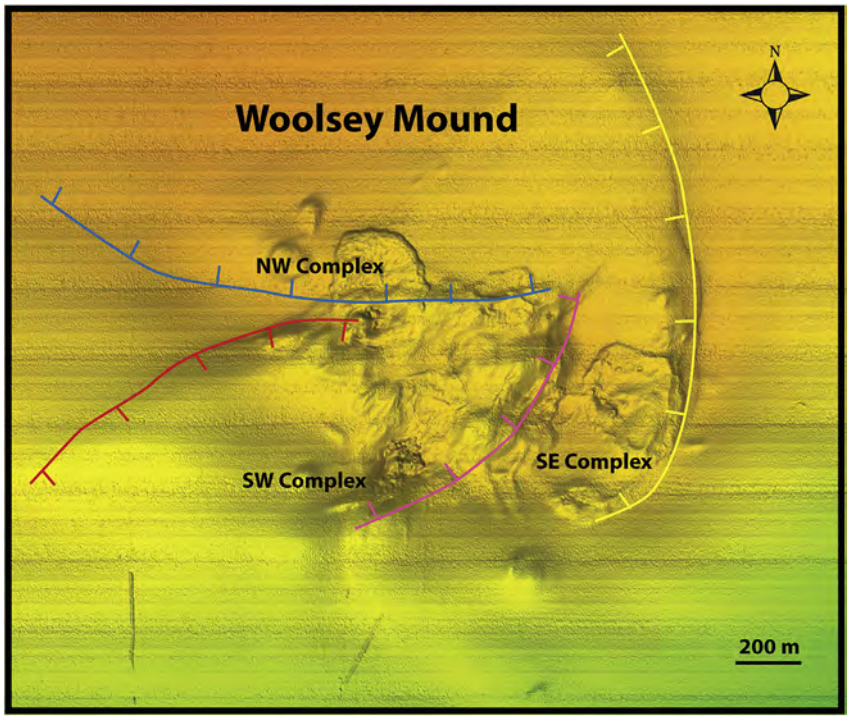

Figure 2. Woolsey Mound seafloor morphology. Woolsey Mound has been subdivided into morphological units [Macelloni et al., 2010] the SE, SW and NW crater complexes. Each complex occurs where deep, salt-related faults intersect the seafloor. These master faults are color-coded as Blue, Red, Magenta and Yellow. (For interpretation of the references to color in this figure legend, the reader is referred to the web version of this article.)

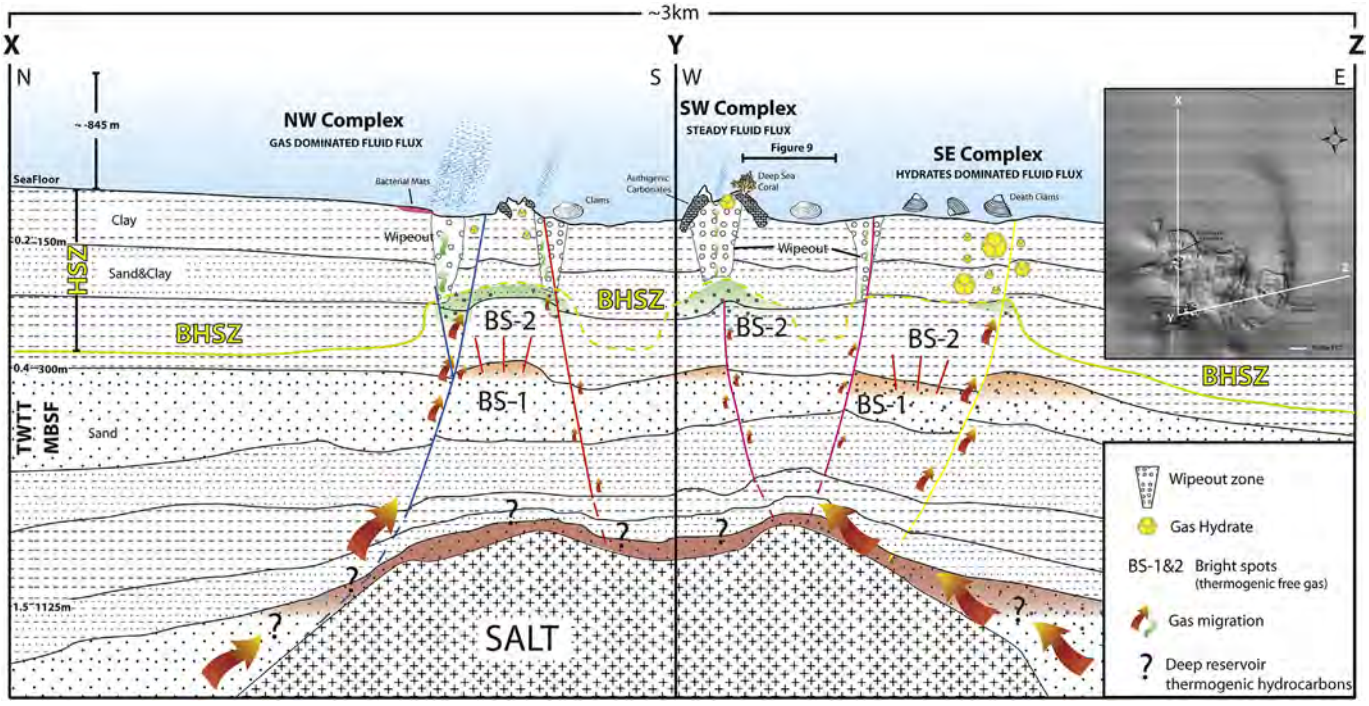

Figure 3. Conceptual model of the Woolsey Mound HSZ and fluid flux regime. Geophysical data from the subsurface [Macelloni et al., 2012] have been combined with observations from the seafloor to understand the mechanism of hydrocarbon gas migration/venting. Each of the three crater complexes is related to specific fault/faults, along which deep-sourced hydrocarbon gas transits. Amplitude anomalies observed on seismic data provide evidence of gas in two shallow subsurface horizons: BS-1 and BS-2. The shallower, BS-2, may mark the base of the HSZ and be directly related to the seafloor venting which varies at each complex. Differences in the spatial distribution of bio-geological processes reflect the responses of the biota to different fluid flux regimes [after Lutken et al., 2011b; Macelloni et al., 2013]. Three mechanisms have been recognized: gas dominated fluid flux at the NW Complex, steady fluid flux at the SW Complex, and hydrate dominated fluid flux at the SE Complex [modified from Macelloni et al., 2013].

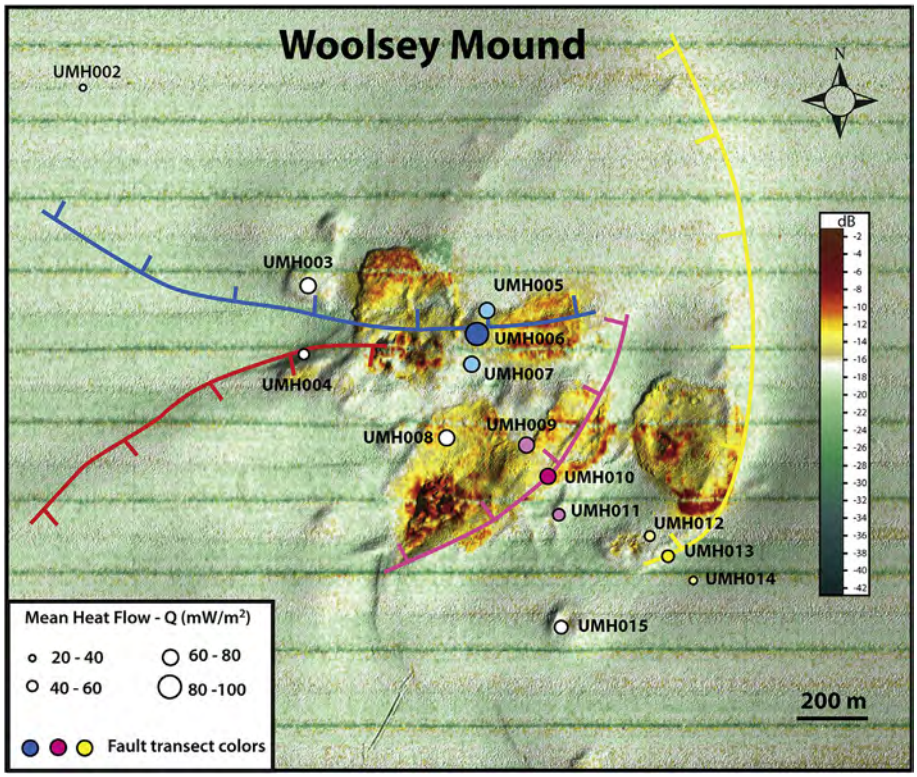

Figure 4. Woolsey Mound heat-flow sites. Site locations are plotted on seafloor backscatter; warmer colors are good indicators of hard-ground [Macelloni et al., 2010] where the probe is unable to penetrate so heat-flow data cannot be recorded. Sites UMH 001–15 were selected as follows: 001 calibration site (outside the map), 002 off-mound site; 003, 004, 015 seafloor pockmarks; 008 a suspected brine pool; 005–007 transect the blue fault; 009–011 transect the magenta fault; 012–014 transect the yellow fault. (For interpretation of the references to color in this figure legend, the reader is referred to the web version of this article.)

core JPC-6 was recovered in 2011 that showed abundant gas in sediments [Simonetti et al., 2013]; transect UMH012-014 crosses the yellow fault at a recently active portion of its exposure, determined by careful inspection of high resolution seismic data.

Descriptions of the heat-flow probe, collection procedure, data analysis and interpretation are reported in Appendix A.

2.2. Hydrates compositional simulator

Over the past several years, Consortium researchers have been developing a new "compositional" simulator to model hydrate formation and dissociation in a complex system, such as that at Woolsey Mound. Unlike existing simulators, this one is designed to accommodate varying conditions of temperature, pressure and salinity as well as multi-gas sources for hydrate formation. A gas hydrate sample recovered at Woolsey Mound in 2002 was found to contain 70% CH4, 7.5% ethane, 15.9% propane, 4.4% i-butane, and 1.1% n-butane [Sassen et al., 2006]. Solid gas hydrate samples were also recovered during a 2011 Jumbo Piston Coring cruise. An average composition for these samples was 79% methane, 11% ethane, 9% propane, and 1% butane [Wilson et al., 2014]. The vent gas samples collected at MC118 in 2002 averaged about 94%–96% methane, 2–3% ethane, and <1% propane [Sassen et al., 2006]. Compared to the vent gas, the solid hydrate is enriched in ethane and propane. A "compositional" (i.e. multi-gas) model is needed to account for the various gas components present in MC118 hydrates, and for what appears as preferential fractionation of higher hydrocarbon gases - ethane and propane - in the hydrate phase.

The hydrate/liquid/gas equilibrium conditions for aqueous/hydrocarbon systems (brine + multi-component gas + hydrate) may be computed using the statistical thermodynamic approach described by Sloan (1998). This procedure has been embodied in a stand-alone computer program called CSMHYD, also available with Sloan (1998). Given the chemical composition of the gas phase (i.e. the mole or mass fraction of various gases in the gas phase) in equilibrium with the liquid and the hydrate, fluid salinity, and temperature, the CSMHYD program yields the equilibrium pressure and the chemical composition of the hydrate phase. The direct use of CSMHYD in a reservoir simulator is impractical because of the unavailability of source code and computational efficiency considerations; therefore we adopted a different approach as described by Garg and Pritchett (2011). The CSMHYD program was exercised extensively to characterize three-phase equilibrium conditions for a three-component hydrocarbon gas (CH_4, C_2H_6 and C_3H_8) in equilibrium with solid hydrate and brine as a function of temperature. The composition of the gaseous phase is specified by the values of two dimensionless parameters H and G:

$$H = (<\text{Ethane}> + <\text{Propane}>)/(<\text{Methane}> + <\text{Ethane}> + <\text{Propane}>), \text{or proportion of non} - \text{methane gas}$$

$$G = <\text{Propane}>/(<\text{Ethane}> + <\text{Propane}>), \text{or proportion of non} - \text{methane gas that is propane}$$

where:

<Methane> = number of moles of CH_4 in the gaseous phase,
<Ethane> = number of moles of C_2H_6 in the gaseous phase, and
<Propane> = number of moles of C_3H_8 in the gaseous phase.

CSMHYD calculations were carried out for temperature $T = 0$ °C, 5 °C, 10 °C, 35 °C, for $H = 0.00, 0.02, 0.04, 0.10$ and for $G = 0, 0.125, 0.25, 0.375, 0.5$ and 1.0. The calculated results were used to formulate mathematical fits to yield equilibrium pressure and the hydrate hydrocarbon composition (molar ratios of CH_4:C_2H_6:C_3H_8) as functions of temperature, salinity, and the values of H and G describing the composition of the free gas in equilibrium with the hydrate and aqueous phases. These mathematical fits have been incorporated into the "compositional hydrate simulator" under development. In the following, the mathematical fits are used to compute the "equilibrium pressure" for the MC118 sites by systematically adjusting the free gas composition in order to reproduce the observed "hydrocarbon composition" of the hydrate sample.

3. Results

3.1. Woolsey Mound heat-flow

The values of heat-flow measured in the survey range from 27.7 to 80.1 mW/m^2. In the mound area they range from 43.8 to 80.1 mW/m^2, averaging 63.5 mW/m^2. The geographical variation of the measured heat-flow is shown in Figure 5. The average conductive heat-flow measured in the mound area is larger than in the surrounding area. The two heat-flow calibration measurements made outside of the mound area were 27.7 (UMH001) and 35.8 (UMH002) mW/m^2. Previous studies in the vicinity of MC118 recovered heat-flow measurements to the southwest of 25 mW/m^2 or less [Blocks MC798, MC 891, TDI-BI, 2001; MC Blocks 852/853, Smith et al., 2014], and to the south, in block MC518 [TDI-BI, 1999], of 37 mW/m^2. This suggests a range of heat-flow in the surrounding areas of 25–37 mW/m^2, and an anomaly in the mound averaging 26–39 mW/m^{2}greater than heat-flow in the surrounding areas. Three heat-flow transits recorded across surface traces of master faults are plotted in Figure 5. The blue fault, in the NW crater; has an average heat flow of 75 mW/m^2, the magenta fault, in the SW crater, of 64.5 mW/m^2 and the yellow fault in the SE crater of 50 mW/m^2. At each heat flow transect, the highest value is found where the fault intersects the seabed while the lowest value occurs on the footwall of the normal fault. We explain this specific heat-flow pattern at the master faults by advective fluid (where "fluid"

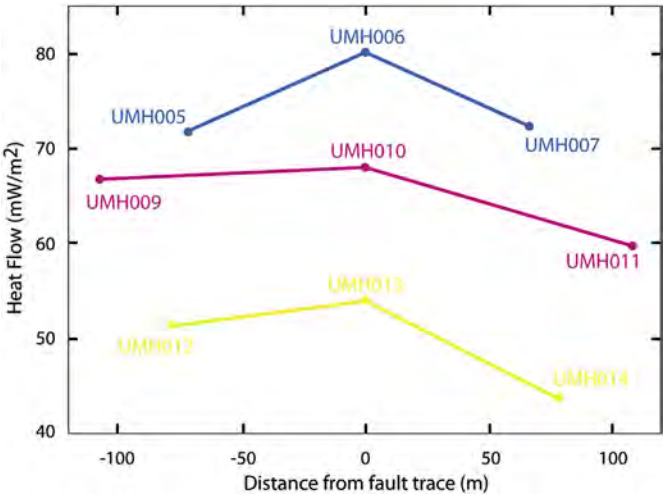

Figure 5. Heat-flow measured on transects crossing seafloor traces where three crestal faults intersect the seafloor. Note that each transect has the highest heat-flow value at the fault plane/trace and that colors correspond to those used for individual fault traces in Figures 2, 3 and 4. (For interpretation of the references to color in this figure legend, the reader is referred to the web version of this article.)

probably is a solution of salt water, hydrocarbon gases, and even oil, i.e. Smith et al., 2014) flow from depth up the master faults, progressing through secondary and tertiary faults and fault zones and eventually through the overlying, surficial sediments. Vertical flow is more easily accomplished than lateral and the many small vertical and near-vertical faults in the vicinity of the Woolsey Mound that are clearly imaged on multiple resolution data datasets [Simonetti et al., 2011; Macelloni et al., 2012; Simonetti et al., 2013] provide accessible pathways for fluids to migrate vertically. In the case of the heat-flow measured across the magenta fault (see Fig. 5) the three values imply that the heat flow is distributed over a broader lateral extent. A close look at the surface bathymetry provides a possible explanation: rather than a single surface trace, this fault is expressed as three parallel traces spaced from 100 m (in the north) to 200 m (in the south, the site of the heat-flow transect) apart. In permeable units confined above by impermeable layers, but intersected by faults, the permeability of the sediments provides accessible lateral flow routes. Most fluid flows, other than ones with enough strength to rupture the bedding, can migrate short distances along the bedding, until they intersect a fault or other features that provide a vertical pathway for fluids migration to the seafloor. High resolution seismic and acoustic data from this area reveal an abundance of closely spaced faults in the shallowest 2–300 m, many with no perceptible vertical displacement, so fluids would not have to migrate very far, laterally, before accessing a vertical migration pathway.

3.2. Computation of BHSZ

At each seafloor site where heat-flow data were collected, the depth of the hydrates stability field has been calculated using the analytical approach reported in Appendix B. Computations were performed for six cases. Cases 1 and 3 are for pure methane hydrate. The gas composition for cases 2 and 4 was selected so as to reproduce the composition of the solid hydrate recovered at Woolsey Mound during the 2011 JPC cruise [Wilson et al., 2014]. Cases 5 and 6 correspond to the solid hydrate composition reported by Sassen et al., (2006). For each gas composition, two fluid salinity distributions are considered, i.e. (1) sea-water salinity (cases 1,3,5), and (2) salinity increasing linearly between sea-water salinity at the sea-floor and saturation salinity at the depth of the salt body. We are aware that the assumption of a constant gradient in NaCl concentration is not correct, in fact the transport of heat and salinity should occur mostly along the faults, and likely in a time variant manner. As evidenced by Smith et al., (2014) in a recent work about heat and chloride vertical transport beneath a vent site at MC852/853, we suspect that salt concentration will be locally very high where and when fluids are transported along faults but will decrease away from the faults and/or during quiescent periods. A nonlinear and time variant salinity gradient would be more appropriate in this geological setting. However, in the absence of subsurface salinity distribution data, a linear approximation of the salinity gradient is a best-possible approximation. Results of the BHSZ computation for the six cases are reported in Tables B1 to B6 in Appendix B.

4. Discussion

4.1. Geothermal regime

To first order, the hydrates stability zone responds to changes in temperature, salinity and pressure, ordered from highest to lowest sensitivity. For example, increasing temperature or salinity in a shallow sedimentary section produces a thinner gas hydrates stability zone. Salt diapirism affects both thermal regime and pore water salinity [Taylor et al., 2000; Ruppel et al., 2005]. Our heat-flow data show that Woolsey Mound has an anomalous thermal regime with respect to the surrounding areas. Figure 6 displays the cumulative histogram of heat-flow values. Along each fault, the heat-flow is markedly different: the blue fault has a heat-flow as much as 150% that of the yellow fault; however, for all the master faults, **the highest heat-flow value corresponds to the measurement taken where the fault intersects the seafloor.**

The heat flow data suggest very focused migration of fluids along the faults confining anomalous chemical and thermal effects to zones within and around on the active conduits. The width of the affected zone is a function of the chemical and thermal diffusivity and possibly duration of flow; seafloor heat flow measurements around seeps are often affected by near-seafloor convection, results from densely spaced pogo transects would contribute more to our understanding of the true mechanism of thermal diffusivity [Kawada et al., 2014], though we have no such component in this study.

We find a direct correspondence between “inferred” fluid flow and measured heat-flow: the yellow fault exhibits the lowest heat-flow as well as the least evidence of open venting from the deep subsurface to the seafloor with few bubble streams and microbial mat as its only biological community. The magenta fault's evidences of fluid flow and measured heat-flow are intermediate. Fluid flow and heat-flow are greatest across the blue fault where the most venting activity has been documented and where the seafloor communities are abundant and diverse. Geothermal data imply that the migration of warm fluids through the fault system is the primary mechanism of geothermal regime modification.

Heat-flow values at the pockmarks are intermediate in value across the mound, implying a control that is independent of the zone of faulting but perhaps a point source to which fluids are being delivered to the seafloor with some regularity in addition to their explosive episodes. The heat-flow measurement at the site of the suspected brine pool is one of the highest in the study. Although not associated with a master fault, this site is very close to the surface trace of another fault seen on high resolution seismic records and supports the hypothesis that the fluid flow is concentrated at the surface expression of major faults. This fault is under investigation as a suspected master fault.

4.2. Dynamics of the hydrate stability zone

Differential migration of fluids, including gases, along different segments of faults creates lateral variability of the geothermal

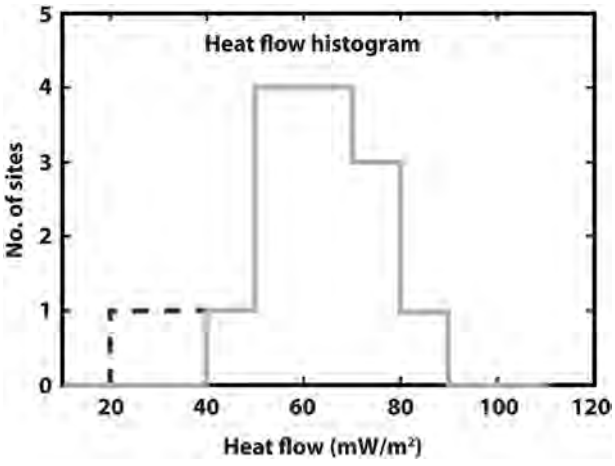

Figure 6. Histogram of the heat-flow values. Values represented by red blocks are those for off-mound sites.

gradient that, ultimately, influences the dynamics of the HSZ. In Figure 7, the subsurface model of Woolsey Mound, as presented by Macelloni et al., [2013], has been integrated with the depth of the base of the hydrate stability zone for cases 3, and 6 as calculated in the section, *Computation of BHSZ*. The two depths represent, respectively, the base of the stability zone assuming pure methane and Woolsey Mound solid hydrates compositions from a sample recovered during a dive of the Johnson SeaLink in 2002 (Sassen et al., 2006). The two depths represent the top-most and lower-most boundaries of the hydrates stability zones resulting from the previous computations. Although Figure 7 is only a schematic representation of the Woolsey Mound hydrates system, the vertical scale (depth) is respected and we believe that this representation adds the "geological dimension" to a traditional hydrates Pressure–Temperature diagram. The cases we show assume a pore-water salinity that varies linearly from 0.035% at sea-floor to saturated salinity at salt-body depth (accurately derived using seismic data). The model takes into account the inhibiting effect that the salt body has on hydrates formation, as evidenced by Ruppel et al., (2005) (see Appendix B and Figure B 1 for details).

Geological and geophysical evidences suggest that the base of hydrates stability at Woolsey Mound lies approximately along the BS-2 horizon of Figure 3 [Macelloni et al., 2012; Macelloni et al., 2013; Simonetti et al., 2013].

The numerical results imply that multiple BHSZs can coexist as a direct consequence of the thermogenic signature of the free gas (see Appendix B for both tabular and graphical representation of the six cases). We observe, however, that the BHSZ curve that best fits the base of the HSZ with the observed geological/geophysical constraints is the one derived from case 6 (the most enriched in propane, the highest order hydrocarbon accommodated by the compositional simulator). The best fit occurs at the SE complex (yellow fault) where the heat-flow is lowest and vent activity at the seafloor is minimal. In particular, along the yellow fault, the depth of the calculated HSZ is consistent with the seismic anomaly referred to as *high frequency scattering* (HFS) which was hypothesized and subsequently confirmed to represent a seismic signature for buried hydrates in fracture porosity [Simonetti et al., 2013]. This anomaly has been observed in discrete packages, both laterally and vertically, throughout the vicinity of Woolsey Mound. The curve derived from case 3 (100% methane, Table B3 in Appendix B) is unrealistic, at least for Woolsey Mound; pure methane hydrate is contrary to the chemical evidence and the BHSZ is too shallow and totally unrelated to either the geological control (faults, sediments type, etc.) or geophysical evidence (bright spots, HFS, etc.). Structure II HSZ (e.g. Gulf of Mexico hydrates) is much thicker than that for Structure I hydrates (e.g. Blake Ridge) and the shoaling effect due to the presence of salt is at least in part diminished by the presence of heavier hydrocarbon gas molecules. Beneath the NW and SW complexes (blue-red and magenta faults), the base of the HSZ diverges from the geological/geophysical model (see Fig. 7). The heat-flow data as well as the bio-geological processes at the seafloor provide evidence that these crater complexes experience continued migration of thermogenic fluids. The NW complex, in

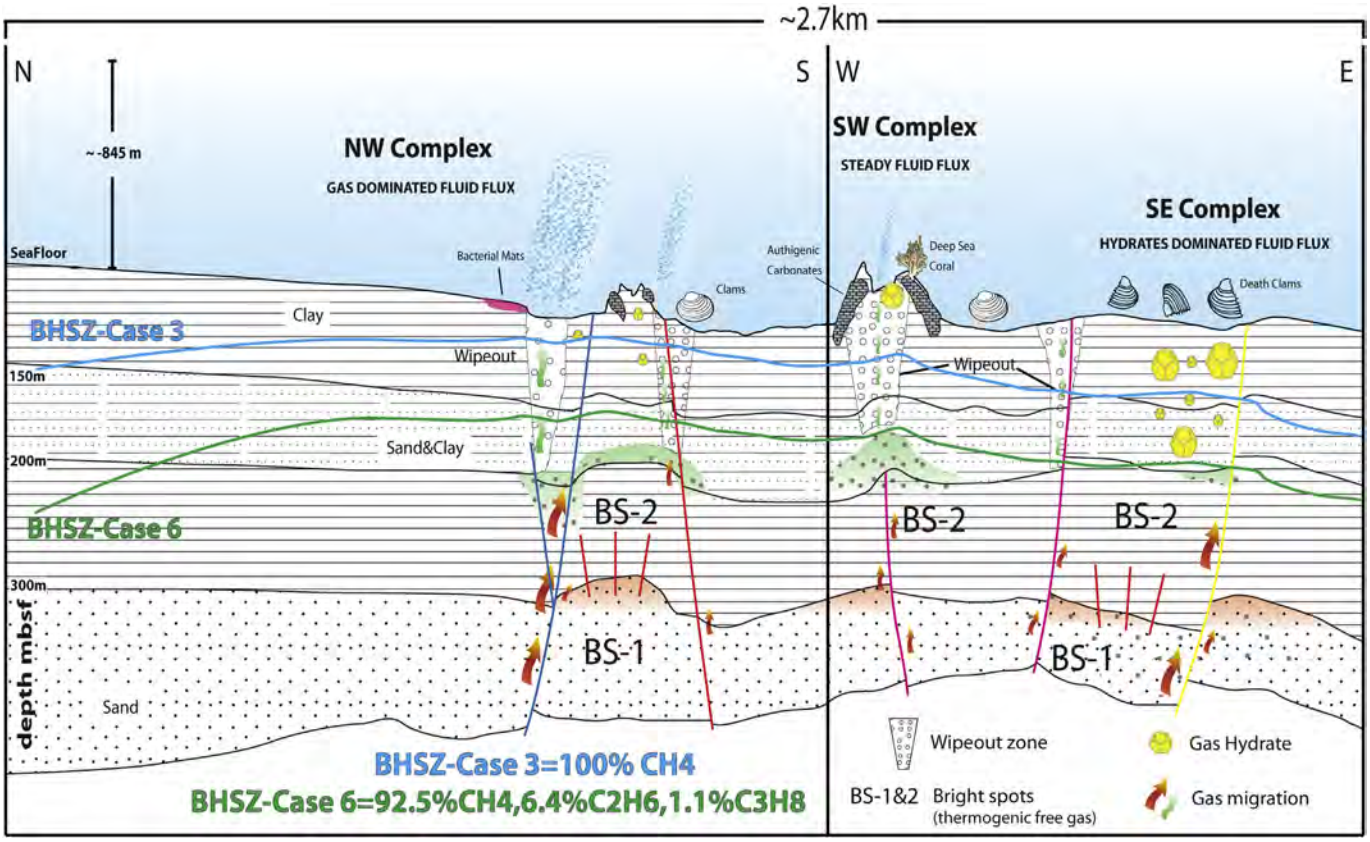

Figure 7. Woolsey Mound hydrates stability depth. The multi-attribute schematic of the Woolsey Mound hydrate system, displayed in Figure 3, has been integrated with the depth(s) of the hydrates stability field derived using our compositional simulator. Only two cases are represented here: Case 3 (pure methane, blue line), and Case 6 (solid hydrate composition is about, 75% methane, 8% ethane, and 17% propane, green line). Salinity is assumed to vary linearly from 0.035% (sea-water salinity) at the seabed to 100% (saturated) at the salt body. The schematic is an idealized representation of a transect passing across the three complexes and intersecting the master faults; however, the vertical scale (depth) is preserved. Theoretically, multiple hydrate stability fields, corresponding to hydrates of differing compositions, are possible; faults segment the stability field. Curve 6 best approximates the base of the hydrate stability zone, geologically and geophysically derived by Macelloni et al., [2012]. (For interpretation of the references to color in this figure legend, the reader is referred to the web version of this article.)

particular, has persistent and occasionally violent fluid expulsion episodes, evidenced by the presence of pockmarks. In this area, the BHSZ ceases to be a boundary that separates solid hydrates from gas, but represents a very dynamic zone where hydrocarbon molecules can coexist in multiple phases (gas, solid hydrate, dissolved in pore fluid), depending upon their lateral distance from a major conduit as suggested by Liu and Fleming (2007). Along the fault conduits, where the heat flow is highest, the stability field can be pushed quite shallow, very close to the seabed.

Solid hydrates sampled at the seafloor, in shallow gravity cores (up to 10 m penetration, west of the NW crater complex) and deeper in jumbo piston cores (up to 18 m penetration, east of the NW crater complex) and very close to the surface trace of the blue fault, have been found to be rich in propane (about 14%). A possible explanation for this could be that hydrate crystallization is similar to mineral crystallization in which a rising, warm, multicomponent fluid will fractionate into solid phase compounds enriched in heavier molecules first. This process, known as fractional crystallization, could supply fluids containing higher order hydrocarbons found at depth to the shallow subsurface where they may be more likely to be dispersed and to form gas hydrate in fractures and voids and lose pressure and heat more rapidly than does the remaining solution. Therefore in a fault-controlled, focused system, not only will hydrate accumulate preferably in fractures and veins along the faults but they will be **genetically enriched** in heavier hydrocarbon molecules that may remain in the system through repeated episodes of formation and dissociation. Although few samples of gas hydrate from Woolsey Mound have been recovered and analyzed, findings are consistent with this hypothesis: the solid hydrates recovered from the vicinity of the master faults have concentrations of higher order hydrocarbons that are greater than those of vent gas and dissolved gases recovered from the complexes (Sassen et al., 2006; Wilson et al., 2014).

It is evident that the hydrate system at Woolsey Mound is controlled by salt-derived fault activity and, in particular, by thermogenic fluids migrating along the faults. Pizzi et al., (2012) and Simonetti et al., (2013) have conducted very accurate analyses of fault movements detectable on high resolution chirp data. They have both found that all master faults have been active in very recent geologic time. Therefore, to explain why the master faults present differences in the heat flow regime, we have to conclude that gas hydrate formation and dissociation vary temporally and temporarily can seal the conduits for thermogenic fluids. Macelloni et al. (2012), have proposed already this mechanism observing the changes of fault related seismic anomalies on time lapse seismic data, and the same concept has been discussed for a long time by others [i.e. Wood et al., 2002]; our heat flow measurements along the faults lead to the same conclusions.

Furthermore, our data suggest that the lateral distribution of hydrates is independent of fault tectonic (macro) activity. Instead the system is regulated by hydrocarbon circulation within the deep petroleum system. Unfortunately this phenomenon is poorly understood and further study, such as permanent monitoring of the fault dynamics, needs to be undertaken.

5. Conclusions

A major goal of the GOM-HRC and seafloor observatory work is to delineate how the hydrate stability zone is impacted by changes in components of the natural environment that determine hydrate stability. These include – but are not limited to – temperature, pressure, salinity, and gas composition. The present study of Woolsey Mound in the northern Gulf of Mexico, illustrates that fault-controlled, thermogenic hydrates systems present a very complex geothermal field that heavily impacts the hydrate stability zone. The three master faults – yellow, magenta and blue – whose vertical extent is traced from the top of salt to the seafloor and whose traces were traversed with heat-flow transects, all showed peak heat-flow directly over the fault. Heat-flow on the flanks, in all cases, was diminished but still elevated over that of the surrounding seafloor, with the multiple-seafloor trace magenta fault showing the greatest spread of heat-flow. A high-resolution heat-flow study, therefore, could be expected to identify open faults, including secondary faults and fault zones along the fault trace transporting fluids from depth to the seafloor. Furthermore, heat-flow data, combined with an accurate knowledge of the geology (particularly the salt position) and gas hydrate composition can be used to constrain, physically, the depth of the hydrate stability field. This depth has been calculated using the phase equilibrium equation in a compositional simulator, and results have shown that as percentage of non-methane gases increases, so does the thickness of the HSZ. Therefore in salt-influenced thermogenic systems, not only is the inhibition process of hydrates formation mitigated by the presence of heavier molecule hydrocarbons, but also, thermogenic gas hydrates can support multiple stability fields. Geothermal data also provide evidence that, within the fluid conduits and in the presence of high activity, the hydrate stability field waxes and wanes and can shoal up to the seafloor. Solid hydrates, enriched in non-methane molecules, can form in fractures and veins near the conduits as a result of rapid loss of temperature and pressure. This process might be physically and chemically analogous to that known as fractional crystallization occurring when warm multicomponent magma fluid rises along faults and fractures derived from volcanic activity and is cooled and crystallized instantaneously upon contact with the host rock of radically different composition and temperature.

Acknowledgments

This paper is dedicated to the memory of Dr. Thomas Martin McGee, who initiated hydrates research at the University of Mississippi and greatly contributed to this study.

The Authors are very grateful to TDI-Brooks, International and the crew of R/V *Geoexplorer*.

This project has been supported by Gulf of Mexico Hydrates Research Consortium through funds provided by DOI BOEM (Grant # CA M08AC12912) and DOE National Energy Technology Laboratory (Award # DG-FC26-06NTA2877), Laura Lapham was partially supported by UMCES contribution #4964.

Appendix A

During 29–30 March, 2012, TDI-Brooks International collected geothermal data at 15 sites aboard the R/V GEOEXPLORER. Two of the sites, one in deeper water, were outside of the mounds area (Fig. A1). A 5.5-m Lister type heat flow probe [Lister, 1979; Hyndman et al., 1979] without acoustic telemetry was used for all of the measurements. The eleven temperature sensors were spaced at 0.5-m intervals. All measurements, except site 15, were single measurements.

Before each measurement, the probe was held at a constant water depth, several meters above the seafloor, in order to intercalibrate the temperature sensors. Above the mounds area, there was a 4.8 mK/m vertical temperature gradient in the water, and even above the deepest site, at a water depth of 1062 m, there was a gradient of 4.0 mK/m. Also, at many sites, the depth during the hold changed significantly, probably due to ship's motions. Consequently a single intercalibration obtained from the best sites, was used for all sites. Corrections for the temperature gradient in the water were applied afterwards.

Figure A2 displays all of the thermal conductivities measured at every site. Of the total of 176 measurements, there were 11 with values greater than 1.1 W/m K. The highest of these high values must be incorrect, or the probe would not penetrate the sediments. They are caused by quasi-horizontal fluid flows in the sediments removing some of the heat from the heat pulse used to make the measurement. The average value of thermal conductivity measured varied from site to site, from 0.954 to 1.066 W/m K. It is possible that smaller amounts of fluid flow are increasing slightly the measured thermal conductivity at many places; the values for sites 1 and 2 outside the mounds area are lower than the other sites.

The heat flow at each site was determined using a Bullard plot, a plot of temperature vs. integrated thermal resistance from the uppermost sensor nearest the seafloor downward. Figure A3 is the Bullard plot for site 4. Note that the thermal depth is relative to the uppermost sensor on the probe, somewhere below the seafloor. Often there is a slight disturbance near the seafloor, likely due to a recent change in bottom water temperature. The temperatures at all of these sites exhibited a perturbation in the upper 1–2 m consistent with a recent warming of the bottom water. The number of sensors used to determine the heat flow, always the deepest ones, varied between 5 and 9, out of the total of 11 sensors.

At site 15 the difference between the averages of the repeated thermal conductivity measurements was 0.2%, but the two measured heat flows differed by 3.8%. Given the disturbed nature of the site, the heat flow might differ by this amount over a few meters.

The measured heat-flow at the 13 sites within the mounds area varied between 43.8 and 80.1 mW/m^2. Outside the area, the heat-flow at the nearest site was 35.8 mW/m^2, and it was 27.7 mW/m^2 at the more distant site.

Table A
Average measured values for each station (WGS84).

Station	Lat	Lon	Depth (m)	BWT (°C)	Q ($^2_{mW/m}$)	Tilt (°)	No. of sensors	k (W/m K)
UMH001	28.810273	−88.517913	1062	5.07	27.7	2.1	7 of 11	0.894
UMH002	28.861978	−88.501296	877	5.63	35.8	1.1	8 of 11	0.944
UMH003	28.856000	−88.495696	888	5.55	53.7	1.4	8 of 11	0.954
UMH004	28.857498	−88.495548	889	5.54	63.5	2	8 of 11	0.996
UMH005	28.857000	−88.490815	895	5.54	71.8	3.3	8 of 11	0.965
UMH006	28.856406	−88.491156	898	5.42	80.1	2.9	5 of 11	1.039
UMH007	28.855700	−88.491218	894	5.54	72.4	1.5	7 of 11	1.024
UMH008	28.854050	−88.491806	894	5.52	75.7	5	7 of 11	1.032
UMH009	28.853905	−88.489731	896	5.58	65.9	3.1	8 of 11	0.989
UMH010	28.853145	−88.489061	897	5.62	67.9	3.3	8 of 11	1.013
UMH011	28.852190	−88.488760	894	5.57	59.8	4.1	7 of 11	0.991
UMH012	28.851873	−88.486553	897	5.45	51.4	2.9	8 of 11	0.979
UMH013	28.851343	−88.485986	901	5.53	53.9	3	7 of 11	1
UMH014	28.850800	−88.485311	902	5.46	43.8	1.3	8 of 11	0.968
UMH015a	28.849691	−88.488811	914	5.39	67	4.9	5 of 11	1.065
UMH015b	28.849691	−88.488811	914	5.44	64.1	2.2	5 of 11	1.067

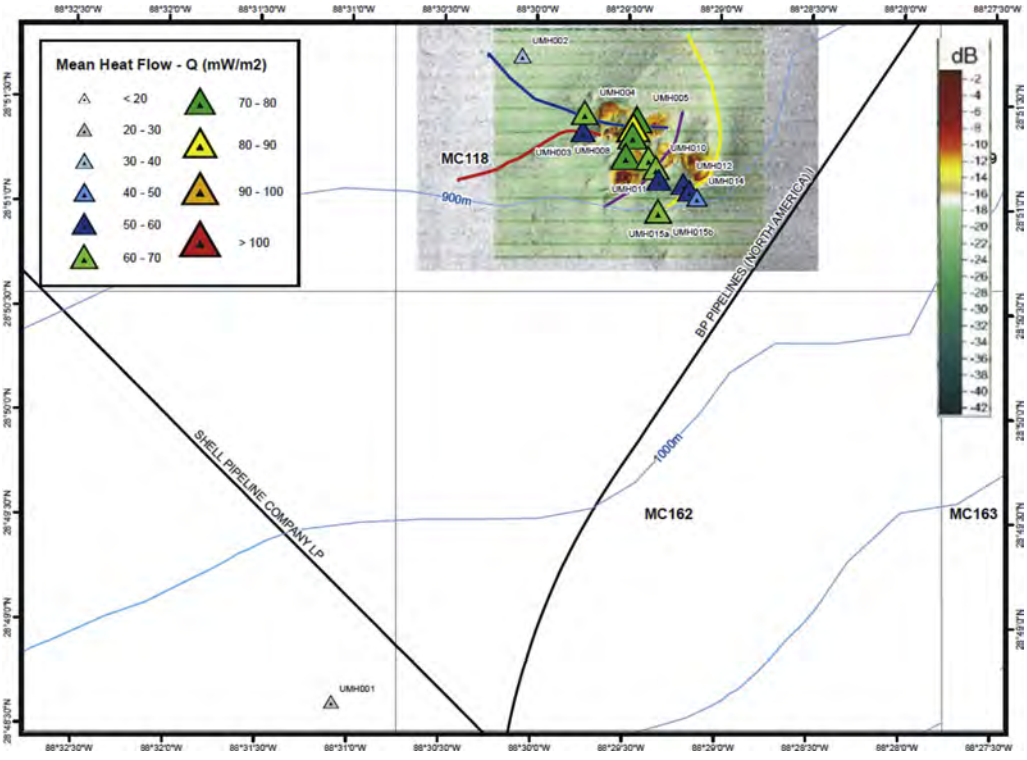

Figure A1. Heat flow measurements sites, included the calibration site UMH001.

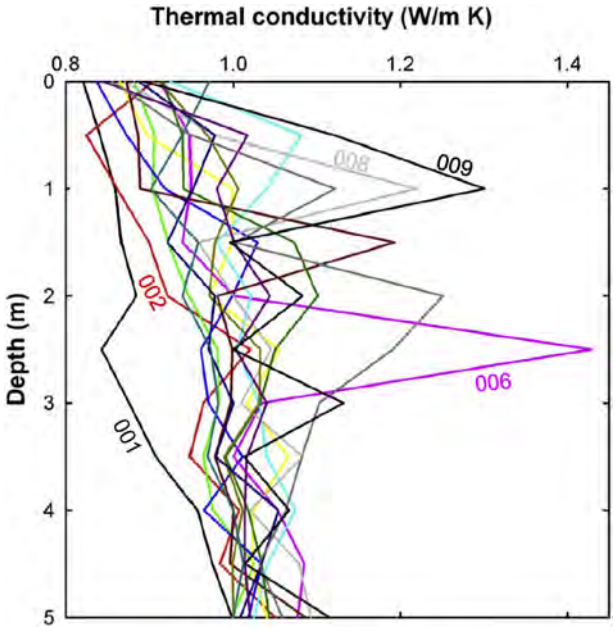

Figure A2. Measured thermal conductivities for each site, as a function of the depth; the depth is relative to the uppermost sensor in the probe.

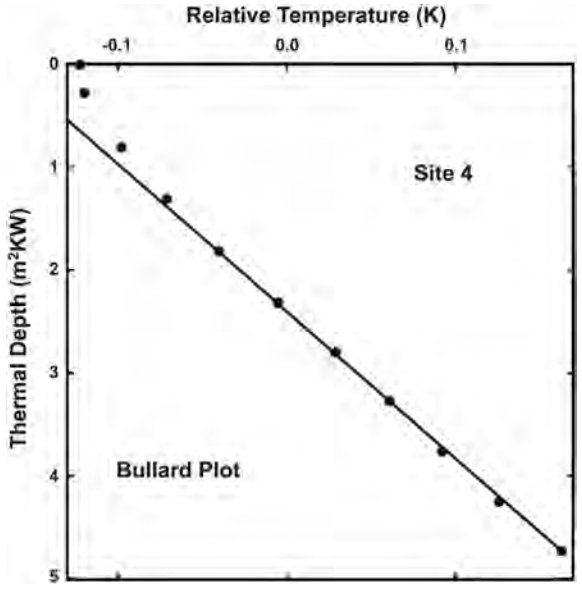

Figure A3. A Bullard plot for site 4 – a typical plot. The inverse of the slope is the heat flow.

Appendix B. Computation of the base of the Hydrate Stability Zone

The TDI-Brooks report lists the seafloor temperatures for all 15 heat-flow sites. In addition; we have the following data, derived from seismic and acoustic surveys, for the 14 sites within Woolsey Mound:

Table B
Geothermal gradient

Heat flow site	Geothermal gradient (°C/Km)	Salt depth (m)	Water depth (m)
002	37.65	−2076	−867
003	56.02	−1405	−880
004	63.48	−1463	−882
005	74.13	−1306	−885
006	76.82	−1328	−889
007	70.43	−1333	−885
008	73.08	−1323	−884
009	66.36	−1314	−886
010	66.76	−1341	−889
011	60.07	−1354	−885
012	52.23	−1437	−888
013	53.63	−1490	−891
014	44.97	−1546	−893
015	62.64	−1457	−902

The temperature at a depth z below the sea-floor is given by:

$$T = T_0 + z \cdot \frac{dT}{dz},$$

where

T_0 = temperature at sea-floor
$\frac{dT}{dz}$ = temperature gradient.

It is assumed that water is saturated with salt at the depth D of the salt body. The saturated salinity S_m is given by:

$$S_m = 0.26218 + T_D\left(7.2 \times 10^{-5} + 1.06 \times 10^{-6} T_D\right)$$

where

S_m = maximum salinity (= amount of dissolved salt/(water + dissolved salt))
T_D = temperature at depth D.

For the preliminary calculations presented hereunder, a linear salinity gradient was assumed between the sea-floor salinity S_0(= 0.035) and the salinity S_m at the salt horizon. Thus the salinity at a depth z below the sea-floor becomes:

$$S = S_0 + z(S_m - S_0)/D.$$

The fluid pressure P at a depth z below the sea-floor is computed using the following equation:

$$P = P_0 + 9.8 \int_0^z \rho dz,$$

where

P_0 = liquid pressure at sea-floor

$$\rho = \rho_0 \times \exp(c \times P)$$
$$\rho_0 = 999.923(1. + 0.81S) \times \exp\left(-(T-4)^2/(13100 + 900T)\right)$$
$$c = \left(4.4 \times 10^{-10} + 2(T-55)^2 \times 10^{-14}\right)/(1. + 2.6S)$$

Within the hydrate stability zone, liquid pressure P exceeds the equilibrium pressure P_{eq}; at the base of the hydrate stability zone, P equals P_{eq}. To compute the depth to the bottom of the hydrate

stability zone, we consider a small space interval dz (say = 0.1 m), and starting at sea-floor proceeded as follows for each dz:

Compute new value of z.

Compute T, S and P corresponding to z.

Given T, S and the free gas composition, use correlations (see Data and Methods) to compute P_{eq} and hydrate composition.

If $P > P_{eq}$, return to step 1. Otherwise, z approximately (within dz) equals the depth to the bottom of the hydrate stability zone.

Table B1
Case 1: Free Gas: 100% methane

Uniform salinity = 0.035							
Site	Temp @ BHSZ (deg C)	BHSZ depth (m below sea-floor))	Equilibrium pressure @ BHSZ (bars)	Liquid pressure @ BHSZ (bars)	Mole fraction of methane in hydrate	Mole fraction of ethane in hydrate	Mole fraction of propane in hydrate
2	11.4507	154.6000	103.1810	103.1550	1.0000	0.0000	0.0000
3	11.0736	98.6000	98.8356	98.8105	1.0000	0.0000	0.0000
4	10.9739	85.6000	97.7247	97.6988	1.0000	0.0000	0.0000
5	10.8774	72.0000	96.6636	96.6275	1.0000	0.0000	0.0000
6	10.9126	71.5000	97.0496	96.9836	1.0000	0.0000	0.0000
7	10.9138	76.3000	97.0626	97.0622	1.0000	0.0000	0.0000
8	10.8841	73.4000	96.7369	96.6682	1.0000	0.0000	0.0000
9	10.9684	81.2000	97.6643	97.6581	1.0000	0.0000	0.0000
10	10.9942	80.5000	97.9496	97.8902	1.0000	0.0000	0.0000
11	11.0544	91.3000	98.6206	98.5781	1.0000	0.0000	0.0000
12	11.2580	111.2000	100.9320	100.8950	1.0000	0.0000	0.0000
13	11.2416	106.5000	100.7440	100.7230	1.0000	0.0000	0.0000
14	11.4995	134.3000	103.7610	103.7370	1.0000	0.0000	0.0000
15	11.2142	92.5000	100.4290	100.4220	1.0000	0.0000	0.0000

Table B2
Case 2: Free Gas: 94.4% methane, 5.2% ethane, 0.4% propane.

Uniform salinity = 0.035							
Site	Temp @ BHSZ (deg C)	BHSZ depth (m below sea-floor))	Equilibrium pressure @ BHSZ (bars)	Liquid pressure @ BHSZ (bars)	Mole fraction of methane in hydrate	Mole fraction of ethane in hydrate	Mole fraction of propane in hydrate
2	15.1065	251.7000	112.9670	112.9520	0.8024	0.1089	0.0887
3	14.6252	162.0000	105.2130	105.2070	0.7971	0.1105	0.0925
4	14.5034	141.2000	103.3530	103.3090	0.7957	0.1108	0.0934
5	14.3763	119.2000	101.4560	101.3900	0.7944	0.1112	0.0944
6	14.3849	116.7000	101.5830	101.5440	0.7945	0.1112	0.0943
7	14.4212	126.1000	102.1220	102.0870	0.7949	0.1111	0.0940
8	14.3846	121.3000	101.5790	101.5010	0.7945	0.1112	0.0943
9	14.4855	134.2000	103.0840	103.0060	0.7955	0.1109	0.0936
10	14.4924	132.9000	103.1880	103.1770	0.7956	0.1109	0.0935
11	14.5805	150.0000	104.5260	104.5010	0.7966	0.1106	0.0928
12	14.7887	178.8000	107.7730	107.7160	0.7989	0.1099	0.0912
13	14.7651	172.2000	107.3990	107.3510	0.7986	0.1100	0.0914
14	15.0296	212.8000	111.6840	111.6570	0.8016	0.1092	0.0893
15	14.6782	147.8000	106.0340	106.0020	0.7976	0.1103	0.0921

Table B3
Case 3: Free Gas: 100% methane

Salinity varies from 0.035 at sea-floor to saturated salinity at salt depth							
Site	Temp @ BHSZ (deg C)	BHSZ depth (m below sea-floor))	Equilibrium pressure @ BHSZ (bars)	Liquid pressure @ BHSZ (bars)	Mole fraction of methane in hydrate	Mole fraction of ethane in hydrate	Mole fraction of propane in hydrate
2	10.0689	117.9000	99.5727	99.5532	1.0000	0.0000	0.0000
3	9.3762	68.3000	95.8557	95.8303	1.0000	0.0000	0.0000
4	9.5773	63.6000	95.5577	95.5400	1.0000	0.0000	0.0000
5	9.3503	51.4000	94.6130	94.6036	1.0000	0.0000	0.0000
6	9.4300	52.2000	95.0988	95.0905	1.0000	0.0000	0.0000
7	9.3855	54.6000	94.9653	94.9306	1.0000	0.0000	0.0000
8	9.3786	52.8000	94.7020	94.6450	1.0000	0.0000	0.0000
9	9.3094	56.2000	95.2772	95.1995	1.0000	0.0000	0.0000
10	9.4053	56.7000	95.6028	95.5505	1.0000	0.0000	0.0000
11	9.3304	62.6000	95.7683	95.7546	1.0000	0.0000	0.0000
12	9.4247	76.1000	97.4483	97.4453	1.0000	0.0000	0.0000
13	9.5898	75.7000	97.7536	97.6982	1.0000	0.0000	0.0000
14	9.5927	91.9000	99.6088	99.5707	1.0000	0.0000	0.0000
15	9.6607	67.7000	98.0083	97.9921	1.0000	0.0000	0.0000

Table B4
Case 4: Free Gas: 94.4% methane, 5.2% ethane, 0.4% propane.

Site	Salinity varies from 0.035 at sea-floor to saturated salinity at salt depth						
	Temp @ BHSZ (deg C)	BHSZ depth (m below sea-floor))	Equilibrium pressure @ BHSZ (bars)	Liquid pressure @ BHSZ (bars)	Mole fraction of methane in hydrate	Mole fraction of ethane in hydrate	Mole fraction of propane in hydrate
2	12.9642	194.8000	107.5370	107.5010	0.7987	0.1100	0.0913
3	11.8747	112.9000	100.5460	100.4750	0.7937	0.1114	0.0949
4	12.2308	105.4000	99.9150	99.8724	0.7933	0.1115	0.0952
5	11.8633	85.3000	98.2201	98.1277	0.7920	0.1119	0.0961
6	11.9881	85.5000	98.6833	98.5489	0.7924	0.1118	0.0958
7	11.9069	90.4000	98.7031	98.6519	0.7924	0.1118	0.0958
8	11.9072	87.4000	98.2499	98.2402	0.7921	0.1119	0.0961
9	11.7515	93.0000	99.1430	99.0331	0.7927	0.1117	0.0956
10	11.8888	93.9000	99.4622	99.4205	0.7929	0.1116	0.0954
11	11.7752	103.3000	100.0110	99.9964	0.7933	0.1115	0.0951
12	11.8847	123.2000	102.3930	102.3580	0.7951	0.1110	0.0939
13	12.1319	123.1000	102.6720	102.6290	0.7953	0.1110	0.0938
14	12.0706	147.0000	105.3700	105.3200	0.7972	0.1104	0.0924
15	12.2227	108.6000	102.2900	102.2410	0.7950	0.1111	0.0940

Table B5
Case 5: Free Gas: 92.5% methane, 6.4% ethane, 1.1% propane.

Uniform salinity = 0.035							
Site	Temp @ BHSZ (deg C)	BHSZ depth (m below sea-floor))	Equilibrium pressure @ BHSZ (bars)	Liquid pressure @ BHSZ (bars)	Mole fraction of methane in hydrate	Mole fraction of ethane in hydrate	Mole fraction of propane in hydrate
2	16.7029	294.1000	117.2690	117.2240	0.7586	0.0812	0.1602
3	16.1882	189.9000	108.0570	108.0180	0.7526	0.0812	0.1663
4	16.0586	165.7000	105.8660	105.7770	0.7510	0.0811	0.1678
5	15.9182	140.0000	103.5480	103.4850	0.7494	0.0811	0.1695
6	15.9213	136.7000	103.5990	103.5590	0.7494	0.0811	0.1695
7	15.9707	148.1000	104.4080	104.3030	0.7500	0.0811	0.1689
8	15.9266	142.4000	103.6850	103.6270	0.7495	0.0811	0.1694
9	16.0317	157.5000	105.4170	105.3530	0.7507	0.0811	0.1682
10	16.0412	156.1000	105.5760	105.5140	0.7508	0.0811	0.1680
11	16.1363	175.9000	107.1730	107.1100	0.7519	0.0812	0.1669
12	16.3452	208.6000	110.7790	110.7180	0.7544	0.0812	0.1644
13	16.3204	201.2000	110.3440	110.2730	0.7541	0.0812	0.1647
14	16.5901	247.5000	115.1790	115.1530	0.7573	0.0812	0.1615
15	16.2129	172.3000	108.4800	108.4700	0.7528	0.0812	0.1660

Table B6
Case 6: Free Gas: 92.5% methane, 6.4% ethane, 1.1% propane.

Site	Salinity varies from 0.035 at sea-floor to saturated salinity at salt depth						
	Temp @ BHSZ (deg C)	BHSZ depth (m below sea-floor))	Equilibrium pressure @ BHSZ (bars)	Liquid pressure @ BHSZ (bars)	Mole fraction of methane in hydrate	Mole fraction of ethane in hydrate	Mole fraction of propane in hydrate
2	14.2142	228.0000	110.9690	110.9570	0.7545	0.0812	0.1643
3	12.9558	132.2000	102.6010	102.5050	0.7487	0.0811	0.1702
4	13.3861	123.6000	101.8040	101.7740	0.7481	0.0811	0.1708
5	12.9530	100.0000	99.7157	99.6698	0.7466	0.0810	0.1724
6	13.1020	100.0000	100.1920	100.0680	0.7470	0.0810	0.1720
7	13.0056	106.0000	100.3660	100.2880	0.7471	0.0810	0.1719
8	13.0107	102.5000	99.8419	99.8232	0.7467	0.0810	0.1723
9	12.8066	108.9000	100.7280	100.7060	0.7473	0.0810	0.1716
10	12.9703	110.1000	101.1710	101.1220	0.7477	0.0811	0.1713
11	12.8385	121.0000	101.9570	101.8600	0.7482	0.0811	0.1707
12	12.9502	143.6000	104.5380	104.5070	0.7501	0.0811	0.1688
13	13.2420	143.8000	104.9080	104.8020	0.7504	0.0811	0.1685
14	13.1454	170.9000	107.8680	107.8370	0.7524	0.0812	0.1664
15	13.3440	126.5000	104.1350	104.1170	0.7498	0.0811	0.1691

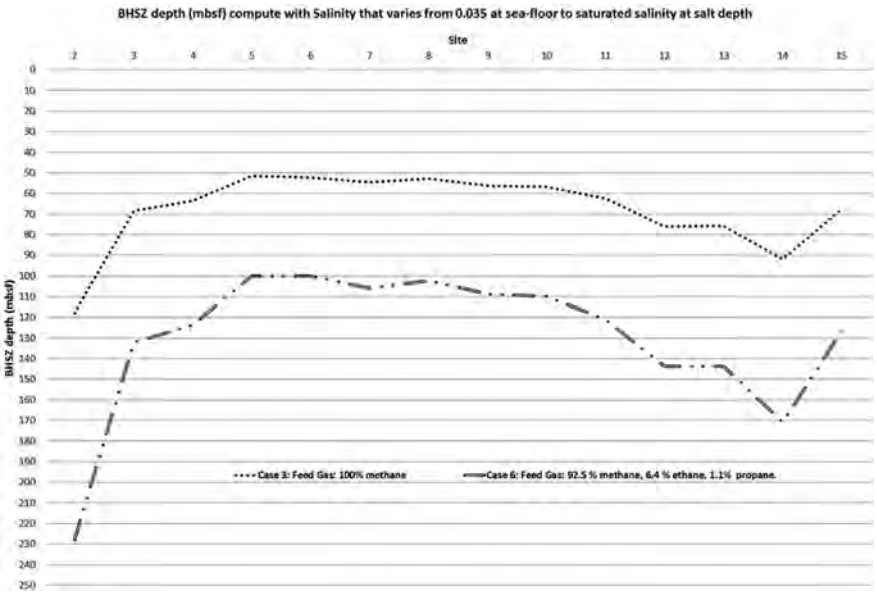

Figure B1. Plot of the depth(s) of the BHSZ computed with salinity that varies from 0.035 at sea-floor to saturated salinity at salt depth of Cases 3and 6 (see Tables B1 to B6).

Appendix C. Supplementary data

Supplementary data related to this article can be found at http://dx.doi.org/10.1016/j.marpetgeo.2014.09.010.

References

Andresen, K.J., Huuse, M., Schodt, N.H., Clausen, L.F., Seidler, L., 2011. Hydrocarbon plumbing system of salt minibasins offshore Angola revealed by three-dimensional seismic analysis. AAPG Bull. 95 (6), 1039–1065.

Brooks, J.M., Cox, H.B., Bryant, W.R., Kennicutt II, M.C., Mann, R.G., Mc Donald, T.J., 1986. Association of gas hydrates and oil seepages in Gulf of Mexico. Org. Geochem. 10, 221–234.

Collett, T., Lee, M., Lewis, R., Mrozewski, S., Guerin, G., Goldberg, D., Cook, A., 2012. Gulf of Mexico gas hydrate joint industry project leg II logging-while-drilling data acquisition and analysis. J. Mar. Petrol. Geol. 34, 41–61.

Cook, A.E., Anderson, B.I., Malinverno, A., Mrozewski, S., Goldberg, D.S., 2010. Electrical anisotropy due to gas hydrate-filled fractures. Geophysics 75 (6), F-173–F-185.

Crutchley, G.J., Berndt, C., Geiger, S., Klaeschen, D., Papenberg, C., Klaucke, I., Maier, C., 2013. Drivers of focused fluid flow and methane seepage at south Hydrate Ridge, offshore Oregon, USA. Geology 41 (5), 551–554.

Dewangan, P., Srirama, G., Ramprasad, T., Ramana, M.V., Jaiswal, P., 2011. Fault system and thermal regime in the vicinity of site NGHP-01-10, Krishna-Godavari basin, Bay of Bengal. Mar. Petrol. Geol. 28, 1899–1914.

Dunbar, J., Gunnell, A., Higley, P., Lagmanson, M., 2010. Seafloor resistivity investigation of methane hydrate distribution in Mississippi Canyon, Block 118, Gulf of Mexico. In: (Expanded Abstract) Symposium on the Application of Geophysics to Engineering and Environmental Problems, vol. 23, pp. 835–844.

Garg, S.K., Pritchett, J.W., 2011. Modeling studies of hydrate Mound, Mississippi Canyon, block 118, gulf of Mexico. In: Proceedings of the 7th International Conference on Gas Hydrates (ICGH 2011), Edinburgh, Scotland, United Kingdom, July 17–21, 2011 (CD-ROM).

Haacke, R.R., Westbrook, G.K., Hyndman, R.D., 2008. Formation of the bottom-simulating reflector and its link to vertical fluid flow. In: Proceedings of the 6th International Conference on Gas Hydrates (ICGH 2008), Vancouver, British Columbia, CANADA, July 6–10, 2008.

Helgerud, M.B., Dvorkin, J., Nur, A., Sakai, A., Collett, T., 1999. Effective wave velocity in marine sediments with gas hydrates: effective medium modeling. Geophys. Res. Lett. 26, 2021–2024.

Hong-Li, L., He, T., Spence, G.D., 2014. North Cascadia heat flux and fluid flow from gas hydrates: modeling 3D topographic effects. J. Geophys. Res. Solid Earth 119 (1), 99–115.

Hornbach, M.J., Ruppel, C., Saffer, D.M., Van Dover, C.L., Holbrook, W.S., 2005. Coupled geophysical constraints on heat flow and fluid flux at a salt diapir. Geophys. Res. Lett. 32, L24617.

Hornbach, M.J., Bangs, N.L., Berndt, C., 2012. Detecting hydrate and fluid flow from bottom simulating reflector depth anomalies. Geology 40 (3), 227–230.

Hutchinson, D.R., Hart, P.E., Ruppel, C.D., Snyder, F., Dugan, B., 2009. Seismic and thermal characterization of a bottom-simulating reflection in the northern Gulf of Mexico. In: Collett, T., Johnson, A., Knapp, C., Boswell, R. (Eds.), Natural Gas Hydrates—Energy Resource Potential and Associated Geologic Hazards, AAPG Memoir, vol. 89, pp. 266–286.

Hyndman, R.D., Spence, G.D., 1992. A seismic study of methane hydrate marine bottom simulating reflectors. J. Geophys. Res. 97, 6683–6698. http://dx.doi.org/10.1029/92JB00234.

Kawada, Y., Tokib, T., Kinoshitac, M., Joshimad, M., Higab, R., Kasayaa, T., Tsunogaie, U., Nishimurad, K., Kisimotod, K., 31 March 2014. Tracing geologically constrained fluid flow pathways using a combination of heat flow measurements, pore water chemistry, and acoustic imaging near the deformation front of the Nankai Trough off the Muroto Peninsula, Japan. Tectonophysics 618, 121–137.

Kvenvolden, K.A., Ginsberg, G.D., Soloviev, V.A., 1993. Worldwide distribution of subaquatic gas hydrates. Geo-Marine Lett. 13 (1), 32–40.

Lapham, L.L., Chanton, J.P., Martens, C.S., Woolsey, J.R., 2008. Microbial activity in surficial sediments overlying acoustic wipe-out zones at a Gulf of Mexico cold seep. Geochem. Geophys. Geosyst. 9 (6).

Liu, X., Fleming, P.B., 2007. Dynamic multiphase flow model of hydrate format marine sediments. J. Geophys. Res. 112 (B03101), 1–23.

Lüdmann, T., Wong, H.K., Konerding, P., Zillmer, M., Petersen, J., Flüh, E., 2004. Heat flow and quantity of methane deduced from a gas hydrate field in the vicinity of the Dnieper Canyon, northwestern Black Sea. Geo-Marine Lett. 24 (3), 182–193.

Lutken, C.B., Macelloni, L., Sleeper, K., D'Emidio, M., McGee, T., Simonetti, A., Knapp, J.H., Knapp, C.C., Caruso, S., Chanton, J., Lapham, L., Lodi, M., Ingrassia, M., Higley, P., Brunner, C., Camilli, R., Battista, B., Short, T., Bell, R., Fietzek, P., 2011a. New discoveries at woolsey Mound, MC118, northern gulf of Mexico. In: Proceedings of the 7th International Conference on Gas Hydrates (ICGH 2011), Edinburgh, Scotland, United Kingdom, July 17–21, 2011.

Lutken, C.B., Simonetti, A., Ingrassia, M., Macelloni, L., Knapp, J.H., Fisher, C., Caruso, S., D'Emidio, M., 2011b. Bio-geophysical classification of seafloor seeps at a carbonate-hydrate mound, northern gulf of Mexico. In: AAPG International Conference and Exhibition, Milan, Italy, October 23–27, 2011. Top 10 Poster Presentation Award.

MacDonald, I.R., Guinasso, N.L., Sassen, R., Brooks, J.M., Lee, L., Scott, K.T., 1994. Gas hydrates that breaches the sea-floor on the continental slope of Gulf of Mexico. Geology 22, 699–702.

Macelloni, L., Caruso, S., Lapham, L., Lutken, C., Brunner, C., Lowrie, A., 2010. Spatial distribution of seafloor bio-geological and geochemical processes as proxy to evaluate fluid-flux regime and time evolution of a complex carbonate/hydrates mound, northern Gulf of Mexico. Gulf Coast Assoc. Geol. Soc. Trans. 60, 461–480.

Macelloni, L., Simonetti, A., Knapp, J.H., Knapp, C.C., Lutken, C.B., Lapham, L., 2012. Multiple resolution seismic imaging of a shallow hydrocarbon plumbing system, Woolsey Mound, Northern Gulf of Mexico. J. Mar. Petrol. Geol. 38, 128–142.

Macelloni, L., Brunner, Charlotte A., Caruso, L., Lapham, L., Lutken, C.B., D'Emidio, M., 2013. Spatial distribution of seafloor bio-geological and geochemical processes

as proxies of fluid flux regime and evolution of a carbonate/hydrates complex, northern Gulf of Mexico. Deep Sea Res. Part I 74, 25–38.
McGee, T.M., 2006. A seafloor observatory to monitor gas hydrates in the Gulf of Mexico. Lead. Edge 25, 644–647.
Pizzi, M., Macelloni, L., Lutken, C.B., D'Emidio, M., March 18–23, 2012. Temporal Evolution of MC118 Woolsey Mound Seep Activity: Constraints from Analysis of Small-scale Salt-induced Sediment Deformation. GRC "Natural Gas Hydrates System", Ventura, CA.
Ruppel, C., Dickens, G.R., Castellini, D.G., Gilhooly, W., Lizarralde, 2005. Heat and salt inhibition of gas hydrate formation in the northern Gulf of Mexico. Geophys. Res. Lett. 32, L04605 the northern Gulf of Mexico continental slope, Geo-Marine Letters, v. 18, pp. 267–276.
Sassen, R., Losh, S., Cathles, L., Roberts, H., Whelan, J.K., Mikov, A.V., Sweet, S.T., Defretias, D.A., 2001. Massive vein-filling gas hydrate: relation to ongoing gas migration from the deep subsurface Gulf of Mexico. Mar. Petrol. Geol. 18, 551–560.
Sassen, R., Roberts, H.,H., Jung, W., Lutken, C.,B., DeFreitas, D.,A., Sweet, S.,T., Guinasso Jr., N.,L., 2006. The Mississippi Canyon 118 Gas hydrate site: a complex natural system. OTC Paper #18132. In: Offshore Technology Conference, Houston, TX.
Shedd, W., Boswell, R., Frye, M., Godfriaux, P., Krame, K., 2012. Occurrence and nature of "bottom simulating reflectors" in the northern Gulf of Mexico. Mar. Petrol. Geol. 34, 31–41.
Singh, S.C., Minshull, T.A., Spence, G.D., 1993. Velocity structure of a gas hydrate reflector. Science 260, 204–207.
Simonetti, A., Knapp, J.H., Knapp, C.C., Macelloni, L., Lutken, C.B., 2011. Defining the hydrocarbon leakage zone and the possible accumulation model for marine gas hydrates in a salt tectonic driven cold seep: examples from Woolsey Mound, MC118, northern Gulf of Mexico. In: Proceedings of the 7th International Conference on Gas Hydrates (ICGH 2011), Edinburgh, Scotland, United Kingdom, July 17–21, 2011.
Simonetti, A., Knapp, J.H., Sleeper, K., Lutken, C.B., Macelloni, L., Knapp, C.C., 2013. Spatial distribution of gas hydrates from high-resolution seismic and core data, woolsey Mound, gulf of Mexico. J. Mar. Petrol. Geol. 44, 21–33.
Smith, A.J., Flemings, P.B., Fulton, P.M., 2014. Hydrocarbon flux from natural deep-water gulf of Mexico vents. Earth Planet. Sci. Lett. 395, 241–253.
Sloan Jr., E.D., 1998. Clathrate Hydrates of Natural Gases. Marcel Dekker Inc., New York, pp. 703–741.
Sloan, E.,D., Koh, C., 2008. Clathrate Hydrates of Natural Gases, third ed. CRC Press., p. 721
Taylor, M.H., Dillon, W.P., Pecher, I.A., 2000. Trapping and migration of methane associated with the gas hydrate stability zone at Blake Ridge Diapir. Mar. Geol. 164, 79–89.
Vanneste, M., Guidard, S., Mienert, J., 2005. Bottom simulating reflections and geothermal gradients across the western Svalbard margin. Terra Nova 17 (6), 510–516.
Wilson, R., Macelloni, L., Simonetti, A., Chanton, J., Knapp, J.H., Lapham, L., Lutken, C.B., Sleeper, K., Brunner, C., Martens, C., D'Emidio, M., 2014. Subsurface methane sources and migration pathways within a gas hydrate mound system, Gulf of Mexico. Geochem. Geophys. Geosyst. 15 (1), 89–107.
Wood, W.T., Gettrust, J.F., Chapman, N.R., Spence, G.D., Hyndman, R.D., 2002. Decreased stability of methane hydrates in marine sediments owing to phase-boundary roughness. Nature 420, 656–660.

Appendix A References

Lister, C.R.B., 1979. The pulse-probe method of conductivity measurement. Geophys. J. R. Astron. Soc. 57, 451–461.
Hyndman, R.D., Davis, E.E., Wright, J.A., 1979. The measurement of marine geothermal heat flow by a multi-penetration probe with digital acoustic telemetry and in situ thermal conductivity. Mar. Geophys. Res. 4, 181–205.